A New Model and Analysis of Orthogonal Machining With an Edge-Radiused Tool

Jairam Manjunathaiah

William J. Endres

Department of Mechanical Engineering and
Applied Mechanics,
University of Michigan,
Ann Arbor, MI 48109-2125

A new machining process model that explicitly includes the effects of the edge hone is presented. A force balance is conducted on the lower boundary of the deformation zone leading to a machining force model. The machining force components are an explicit function of the edge radius and shear angle. An increase in edge radius leads to not only increased ploughing forces but also an increase in the chip formation forces due to an average rake angle effect. Previous attempts at assessing the ploughing components as the force intercept at zero uncut chip thickness, which attribute to the ploughing mechanism all the changes in forces that occur with changes in edge radius, are seen to be erroneous in view of this model. Calculation of shear stress on the lower boundary of the deformation zone using the new machining force model indicates that the apparent size effect when cutting with edge radiused tools is due to deformation below the tool (ploughing) and a larger chip formation component due to a lower shear angle. Increases in specific energy and shear stress are also due to shear strain and strain rate increases. A consistent material behavior model that does not vary with process input conditions like uncut chip thickness, rake angle and edge radius can be developed based on the new model. [S1087-1357(00)01302-2]

Introduction

To achieve the edge strength needed to cut materials, slightly negative rake angles are used with hones and T-lands applied to the cutting edges. The presence of a sizeable edge demands that machining force models account for the geometry of the edge. At the same time, the effects of the ''natural'' sharpness of a cutting edge has to be taken into account in machining force models, particularly at low uncut chip thickness.

In a recent study of commercial cutting inserts by Schimmel et al. [1], it was shown that edge radius varies significantly along an edge (up to 20 μm on a tool of 50 μm nominal edge hone) and also from edge to edge (up to 25 μm on a tool of 50 μm nominal edge hone) and insert to insert. Orthogonal cutting tests presented in that paper showed that this variation could cause an estimated 20–40 percent variation in machining forces, particularly at smaller values of uncut chip thickness.

The metal cutting literature reflects many attempts at capturing the effects of the edge hone on machining forces and process mechanics. Qualitative explanations—such as an increase in edge radius causes an increase in machining forces, which is attributed to a higher proportion being the ploughing forces—are most frequently used. There have been many attempts at modeling the ploughing forces. Unfortunately, these models do not *explicitly* account for the edge geometry and, hence, are limited in their application.

The aim of this work is to develop a machining model that explicitly includes the effects of edge radius without resorting to the highly computational finite element method or the complexities of rigorous slip line analysis. Presented here is the formulation of the machining model and its use to analyze data obtained with careful control and documentation of edge radius. Included as well is a discussion of the experimental results in light of the presented model.

Contributed by the Manufacturing Engineering Division for publication in the JOURNAL OF MANUFACTURING SCIENCE AND ENGINEERING. Manuscript received Dec. 1997; revised Sept. 1999. Associate Technical Editor: K. Ehmann.

Background

It is well understood that the plastic deformation zone, even for fairly sharp tools, is thick and extends below the cutting edge. The size of the plastic zone is a function of the edge radius as well as the rake angle of the tool. Increasing the edge radius for a fixed uncut chip thickness leads to a dilation of the shear zone and a larger zone of deformation below the tool [2]. This observation is very similar to the one made by Kita et al. [3] and Makino and Usui [4] regarding negative rake cutting. This brings forth the idea of an average or equivalent rake angle [5,6] to account for the apparent negative rake introduced by the edge hone. The model of Manjunathaiah and Endres [5] considers a tool with an edge radius to behave with an average rake angle that is obtained by connecting the base of the tool with the point on the rake face at the level of the free surface (i.e., the height of the point is equal to the uncut chip thickness).

In trying to analyze the effects of the natural sharpness of a cutting tool, both Albrecht [7] and Masuko [8] proposed that ploughing caused by the edge radius of the tool was the second most important energy dissipation mechanism next to shearing. The average rake angle effect is thus related to the ploughing mechanism. There have been other attempts to model the ploughing mechanism and relate it to the edge radius [9–16]. However, none of these works explicitly account for the edge radius. Thomsen et al. [14] proposed that the machining force intercept at zero uncut chip thickness was an approximate estimate of the force required to deform the workpiece, and hence, not available for chip formation. Hsu [12] extrapolated the machining force to a finite uncut chip thickness equal to the edge radius, since he believed that the force should be zero at zero uncut chip thickness. His and others' methods involving machining force intercepts have been known to over-estimate the ploughing forces and have been criticized [17].

A model presented by Abdelmoneim and Scrutton [9] includes the energy spent in deformation. That model is applicable only when cutting at a level of uncut chip thickness that is smaller than the edge radius. Connolly and Rubenstein [18] proposed a force

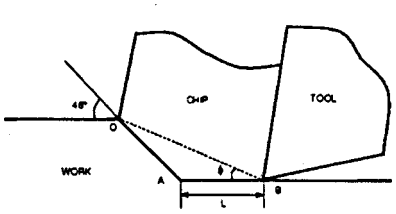

Fig. 1 Connolly and Rubenstein's cutting model

model based on a force balance on the lower boundary of the idealized deformation zone as shown in Fig. 1. The machining force components were written as

$$F_C = (2h + L)S + F_{cl} \tag{1}$$

$$F_T = Lp_m + N_{cl}, \tag{2}$$

where $L = h(\cot\phi - 1)$ describes the deformation in front of the tool, S is the flow stress, p_m is the mean normal stress on the boundary AB, and F_{cl} and N_{cl} are the clearance face forces. The model was validated across a wide variety of experimental conditions while machining with sharp tools. A drawback with the model is that the force components are not modeled as functions of the edge radius and the deformation below the tool was not included. However, the model does represent a good method of understanding machining force data for sharp tools.

Wu [16] modeled the ploughing component of the thrust force as being proportional to the total volume of material displaced by the edge. The ploughing component of the cutting force was then computed to be proportional to the thrust component by a constant coefficient of friction. The magnitude of the ploughing components are critically dependent on the value of the penetration depth p. Unfortunately, there are no reliable methods to predict p. Also, the ploughing mechanism is modeled as being independent of the shearing process, which is questionable. Endres et al. [11] took this idea for modeling the ploughing forces a little further by developing a procedure that would calibrate p based on experimental data and decompose the ploughing components from the total force. Since the procedure was based on an empirical analysis there is no way of ascertaining that the results obtained are correct. Elanayar and Shin [10] modeled the ploughing forces based on frictionless indentation of an elastic half space. The use of frictionless elastic analysis for a plasticity problem in which friction plays an important role seems to diminish the practicality of this analysis. Recently, Waldorf [15] used slip line field analysis to model the process when cutting with an edge bone. Limitations of the analysis include the facts that it is applicable only to tools of zero rake angle, and that no good methods exist to estimate some of the geometry variables needed for the analysis.

In summary, from the literature reviewed here concerning the process mechanics and modeling, it is clear that there are no perfect methods to reliably predict forces when cutting with edge-radiused tools across a wide and practical range of conditions. However, the references cited provide many observations and trends that are very useful in the development of a new cutting model.

The Geometry Model

The idealized geometry of the new process model, displayed in Fig. 2, shows a tool of edge radius r_n removing material of uncut chip thickness h as measured from the bottom of the tool C (same as level D). The flow is assumed to occur without a built-up edge or a stable stagnation zone. Material flowing at the bottom level of the tool passes through point D and rises up to the chip separation point P. The chip separation point P (defined by the separation angle θ, exaggerated in Fig. 2) exists on the radius where the flow separates. The vertical height of point P is taken to be p, which is referred to as the penetration depth. It is obvious that p is a function of both θ and r_n. Since the value of θ is observed from previous works to be less than 60 deg, the arc CP of the tool is approximated by the straight line CP. The rake face of the tool is defined by the average rake angle γ_{avg} instead of the nominal rake angle γ_o. The average rake angle is the angle of the line connecting the flow separation point P and the last point of chip-tool contact [5].

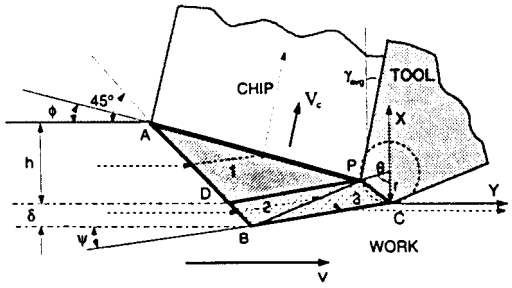

Fig. 2 Geometric model of the cutting process with an edge radius tool

The plastic deformation is assumed to occur in the zone $ABCP$ instead of a shear plane. Material is in a plastic state when it reaches the first line of deformation AB. Material that forms the chip exits the plastic zone at AP, which is similar to the traditional shear plane. Work material that forms the machined surface exits the deformation zone at line BC. Line AB is a plane of maximum shear stress since it is the first line of plastic deformation and hence a slip line. Slip lines always meet a free, unstressed surface at 45 deg, which sets the orientation of line AB. The boundary BC characterizes the deformation below the tool and is inclined at an angle ψ to the horizontal, the value of which could be determined by observing, through experiment, the depth of plastic deformation into the machined surface. The upper boundary of the deformation zone is bounded by the traditional shear plane AP, which is inclined at an angle ϕ to the horizontal, the value of which can be either observed visually or calculated from chip ratios using an average rake angle model. The depth of deformation below the tool, δ, is related to the inclination of the boundary BC as specified by ψ. Such a flow under the tool causes a gradient in the horizontal velocity component, which manifests itself as the distortion of the machined surfaced in the direction of the tool motion.

Placing the origin of the X-Y coordinate system at C, it is possible to derive the coordinates of all other points of interest. The height of the separation point P can be written in terms of the radius r_n and angle θ as $p = r_n(1 - \cos\theta)$. The depth of deformation depends on not only the angle ψ but also the shear angle ϕ and can be derived as

$$\delta = \frac{(h - p)\cot\phi + r_n \sin\theta - h}{1 + \cot\psi}. \tag{3}$$

The lines AB, BC, DP and AP are all lines of velocity discontinuity where the material is assumed to shear instantaneously.

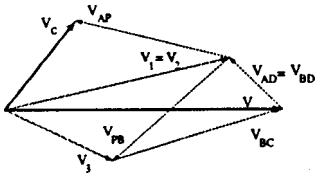

Fig. 3 Velocity hodograph for the new geometric model for orthogonal cutting

They divide the entire deformation zone into three sub-zones ADP, BDP and BCP as shown in Fig. 2. It can be seen that material flowing above the level of h undergoes deformation at the boundary AD such that it flows in a direction parallel to DP with velocity V_1 in zone 1. It undergoes a larger deformation at the upper boundary AP as it flows into the chip at velocity V_c. Material under the base of the tool undergoes shear deformation at BD entering zone 2. The velocity changes from V_2 to V_3 with deformation at BP. Finally, it undergoes deformation at BC such that it exits at the same level and forms the machined surface. This is seen graphically in the hodograph shown in Fig. 3.

Shear Strain and Strain Rate

It can be seen from the hodograph that the velocity of flow in zones 1 and 2 are the same. This velocity is

$$V_1 = \frac{1}{\sqrt{2}\sin(\pi/4+\theta_{PD})} V = V_2 \tag{4}$$

where θ_{PD} is the inclination of the line PD relative to the horizontal. The velocity of the chip is given by

$$V_c = \frac{\sin(\phi+\theta_{PD})}{\sqrt{2}\cos(\gamma_{avg}-\phi)\sin(\pi/4+\theta_{PD})} V. \tag{5}$$

The velocity in zone 3 is

$$V_3 = \frac{\sin\psi}{\sin(\psi+\theta/2)} V. \tag{6}$$

At each of the lines of deformation, the tangential velocities of the shear discontinuities (as indicated by a $*$ superscript) are

$$V^*_{AD} = V^*_{BD} = \frac{\sin\theta_{PD}}{\sin(\pi/4+\theta_{PD})} V, \tag{7}$$

$$V^*_{BC} = \frac{\sin\theta/2}{\sin(\theta/2+\psi)} V, \tag{8}$$

$$V^*_{BP} = \frac{\sin(\theta/2+\theta_{PD})}{\sqrt{2}\sin(\theta/2+\theta_{PB})\sin(\pi/4+\theta_{PD})} V, \tag{9}$$

and

$$V^*_{AP} = \frac{\cos(\gamma_{avg}+\theta_{PD})}{\sqrt{2}\cos(\gamma_{avg}-\phi)\sin(\pi/4+\theta_{PD})} V, \tag{10}$$

where θ_{PB} is the acute angle made by line PB with the horizontal.

Shear Strain. The chip undergoes a shear strain γ_{chip} as it enters boundary AD and later as it exits the boundary AP. This strain can be written as

$$\gamma_{chip} = \frac{V^*_{AD}}{V^n_{AD}} + \frac{V^*_{AP}}{V^n_{AP}} \tag{11}$$

where the superscript n represents the normal component of velocity at the respective boundary. This can be expanded by substituting for the velocity components that can be derived from the hodograph in Fig. 3 as

$$\gamma_{chip} = \frac{\sqrt{2}\sin\theta_{PD}}{\sin(\pi/4+\theta_{PD})} + \frac{\cos(\gamma_{avg}+\theta_{PD})}{\cos(\gamma_{avg}-\phi)\sin(\phi+\theta_{PD})}. \tag{12}$$

Since θ_{PD} is usually small, most of the strain is applied at the boundary AP. In the limit as θ_{PD} goes to zero, this formula is identical to the one obtained in Merchant's shear-plane model.

Similarly, the strain imposed on the material in the machined surface can be written as

$$\gamma_{work} = \frac{V^*_{BD}}{V^n_{BD}} + \frac{V^*_{BP}}{V^n_{BP}} + \frac{V^*_{BC}}{V^n_{BC}}. \tag{13}$$

This strain can be written as

$$\gamma_{work} = \frac{\sqrt{2}\sin\theta_{PD}}{\sin(\pi/4+\theta_{PD})} + \frac{\sin(\theta_{PD}+\theta/2)}{\sin(\theta_{PB}+\theta/2)\sin(\theta_{PB}+\theta_{PD})} + \frac{\sin\theta/2}{\sin\psi\sin(\psi+\theta/2)}. \tag{14}$$

An average strain for the entire deformation zone is approximated by weighting the strains imposed in the chip and the work by their respective deformation volumes:

$$\gamma_{eff} = \frac{v_{chip}\gamma_{chip} + v_{work}\gamma_{work}}{v_{chip}+v_{work}}. \tag{15}$$

Shear Strain Rate. To consider the strain rate effects later, a strain rate averaged across the entire deformation zone $ABCP$ is desired. The strain rate can be obtained by considering the average time it takes for the material to pass through the deformation zone $ABCP$.

The average time taken for material to pass through the deformation zone ADP is given by the ratio of the average distance (equal to half the length of $\overline{PD}$) and velocity V_1. During this time, a strain of γ_{chip} is imposed on the chip. The shear strain rate for the material that goes into the chip is then given by

$$\dot{\gamma}_{chip} = 2V\frac{\gamma_{chip}}{\sqrt{2}\sin(\pi/4+\theta_{PD})\overline{PD}}. \tag{16}$$

The average time taken for material to pass through the deformation zone $BCPD$ is given by the average times to pass through zones 2 and 3. The average times are the ratios of the average distances to pass through the zone ($\overline{PD}/2$ and $\overline{PC}/2$) and the respective velocity in the zone (V_2 and V_3). As previously, the strain rate for the material that passes beneath the tool to form the machined surface can be written as

$$\dot{\gamma}_{work} = 2V\frac{\gamma_{work}}{\sqrt{2}\sin(\pi/4+\theta_{PD})\overline{PD} + \frac{\sin(\psi+\theta/2)}{\sin\psi}\overline{PC}}. \tag{17}$$

In order to obtain a strain rate averaged across the entire deformation zone, we define an effective shear strain rate $\dot{\gamma}_{eff}$. Since different volumes of material are flowing through the two deformation regions ADP and $BCPD$, the effective shear strain rate is computed by weighting the shear strain rates by their respective deformation volumes. This can be written as

$$\dot{\gamma}_{eff} = \frac{v_{chip}\dot{\gamma}_{chip} + v_{work}\dot{\gamma}_{work}}{v_{chip}+v_{work}}. \tag{18}$$

The Force Model

Consider a force balance on the lower boundary (ABC) of the plastic deformation zone of the geometry model. The forces experienced by the work material must be in equilibrium with the forces acting on the tool. Knowing the geometry of the lower boundary of the plastic deformation zone and the stress distribution on the surface, the force components acting on the workpiece can be calculated and set equal to the forces on the tool. This can be done without specifying the upper boundary of the deformation zone. For the principle to be successful, the geometry of and the stress distribution on the lower deformation boundary must be well estimated. Please note that the all the force calculations are performed based on a unit width of the workpiece.

It is necessary, at this point, to consider the stress distribution on the surface ABC. Based on a review of experimentally observed stress distributions on the lower boundary of the shear zone [3,4,19], a typical stress distribution can be described as follows. The shear stress is uniformly distributed over the surface ABC. The normal stress on the lower boundary of the deformation zone

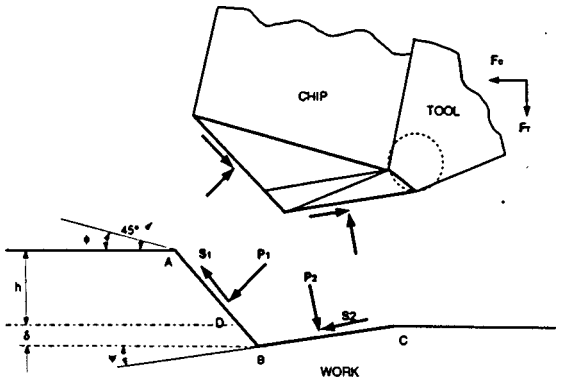

Fig. 4 Force balance on the lower boundary of the shear zone

becomes less compressive away from the free surface. At a point close to the tool, it reverses, turning tensile as it reaches the tool. In view of these observations, it will be assumed that uniformly distributed shear stresses S_1 and S_2 act along AB and BC. It will also be assumed that mean normal stresses P_1 and P_2 act along AB and BC, respectively, as shown in Fig. 4.

The resultant force on surface AB can be written as

$$\hat{F}_{AB}=\frac{1}{\sqrt{2}}(-(S_1+P_1)i+(S_1-P_1)j)\overline{AB}. \tag{19}$$

Similarly, the resultant force on surface BC can be written as

$$\hat{F}_{BC}=((-S_2\cos\psi+P_2\sin\psi)i-(S_2\sin\psi+P_2\cos\psi)j)\overline{BC}. \tag{20}$$

Imposing equilibrium of the chip leads to the equation

$$\hat{F}_{AB}+\hat{F}_{BC}=-F_C i-F_T j. \tag{21}$$

Since AB is a slip line meeting the free surface at 45 deg, as previously mentioned, it follows from slip line field theory that $P_1=S_1$ over the whole surface AB [20]. To avoid a shear stress discontinuity at B, $S_2=S_1$ at B and over the surface BC. Allowing $S_1=S_2=P_1=S$ and separating the orthogonal components in Eq. (21), the cutting and thrust force components can be written as

$$F_C=\sqrt{2}S\overline{AB}-(-S\cos\psi+P_2\sin\psi)\overline{BC} \tag{22}$$

$$F_T=(S\sin\psi+P_2\cos\psi)\overline{BC}. \tag{23}$$

Further, the mean normal stress on BC is considered to be a proportion of the shear stress such that $P_2=kS_2=kS$ where k is defined as a normal stress factor that varies with cutting conditions. Substituting $P_2=kS$ and the geometrical formulations for the lengths $\overline{AB}$ and $\overline{BC}$, the equations for cutting and thrust forces become

$$F_C=2hS+((1+\cot\psi)-(k-1))\delta S \tag{24}$$

$$F_T=(1+k\cot\psi)\delta S. \tag{25}$$

Substituting for δ from Eq. (3) and re-arranging the terms leads to the machining force model

$$F_C=\{(h-p)\cot\phi+h+r_n\sin\theta-(k-1)\delta\}S \tag{26}$$

$$F_T=\{(h-p)\cot\phi-h+r_n\sin\theta+(k-1)\delta\cot\psi\} \tag{27}$$

It is not possible to exactly separate the chip removal and ploughing force terms in Eqs. (26) and (27) since the force balance has been conducted on surface ABC. If such an exact decomposition is desired, the force balance must be conducted on the surface APC. Idealization of the stress distributions on APC is not attempted here. Instead, a comparison is made with the cutting model presented by Connolly and Rubenstein [16] by re-writing Eqs. (26) and (27). Let us define $h'=h-p$ and $L'=h'(\cot\phi-1)$—variables similar to the ones used in their model. The machining force components can then be written as

$$F_C=\{(2h'+L')+r_n\sin\theta+p-(k-1)\delta\}S \tag{28}$$

$$F_T=\{L'+r_n\sin\theta-p+(k-1)\delta\cot\psi\}S. \tag{29}$$

It is now possible to regard the ploughing force as the sum of the force components due to the edge radius and the deformation below the tool allowing Eqs. (28) and (29) to be written as

$$F_C=(2h'+L')S+F_{Cp} \tag{30}$$

$$F_T=L'S+F_{Tp} \tag{31}$$

where

$$F_{Cp}=\{r_n\sin\theta+p-(k-1)\delta\}S \tag{32}$$

$$F_{Tp}=\{r_n\sin\theta-p+(k-1)\delta\cot\psi\}S. \tag{33}$$

Comparing Eqs. (30) and (31) to Connolly and Rubenstein's force model the following observations can be made. The overall nature of the equations are similar in that they contain a chip formation force component and a ploughing force component. Even though the chip formation components of the forces look similar in both cases, the ploughing terms of the new model are not assumed to be a constant. Unlike other models that treat the effects of the edge hone (ploughing) as independent of chip removal, these equations clearly couple the two mechanisms through the shear angle ϕ, on which δ depends as shown in Eq. (3).

The ploughing force components are explicit functions of the edge radius and show implicit dependence on ϕ. A decrease in h/r_n for a given tool leads to a lower average rake angle of the tool due to the negative rake introduced by the edge radius, which in turn leads to a lower shear angle that affects not only the shearing process but also the ploughing process. Based on the new formulation, it is seen why previous attempts at assessing the ploughing forces as the force intercept at zero (or at a finite uncut chip thickness) led to erroneous results. In the force intercept methods, an increase in force due to an increase in edge radius is completely attributed to the ploughing mechanism. On the contrary, in this force model the increase in forces is partly due to an increased chip formation component arising from a smaller shear angle.

Data Analysis and Results

The use of Eqs. (30) and (31) is limited only by the proper estimation of values for θ, ψ, ϕ, S, and k. The first two can be set *a priori* based on the following arguments while the others are computed from experimental data, the discussion of which follows later in detail.

A critical negative rake angle of -75 deg (angle of the tangent to the honed edge) is generally adopted to locate the separation point. This is based on analyses [21,22] and experiments with negative rake angle tools [23]. Thus, θ can be estimated to be 30 deg. It can also be seen that, for a set value of ϕ, the machining force equations are insensitive to the value of θ since it does not significantly alter the lengths of either AB or BC (see Fig. 2). Therefore, a nominal value for θ of 30 deg will be used throughout.

Preliminary investigation of other experimental data has indicated that ψ could well be a constant with uncut chip thickness. Variation of ψ affected the shear stress magnitudes marginally while preserving the same trends. While the value for ψ would best be chosen such that it matches experimentally obtained values for depth of plastic deformation δ, the aforementioned observations led to a constant value of 20 deg being assumed for ψ.

Given assumed values of θ and ψ as noted above, shear stress S and normal stress factor k are obtained by simultaneously solving Eqs. (26) and (27) utilizing known shear angles from cutting tests.

Analysis of two sets of data is presented: analysis of slow speed cutting tests conducted on 70-30 brass in which shear angle was measured visually using *in situ* video, and analysis of cutting data conducted at ''regular'' cutting speeds by Thomsen et al. [14].

Analysis I. Slow speed cutting tests were conducted on 70-30 brass. The cutting and thrust force components from those tests are presented in Figs. 5 and 6. Shear angle data was obtained from visual observation of video images. The normal stress factor and shear stress data calculated under the model presented here are plotted versus uncut chip thickness in Figs. 7 and 8, respectively.

Figure 7 shows that the normal stress factor k is relatively constant across uncut chip thickness at a value around 1.1. This means that the normal stress on the lower boundary of the deformation zone is on an average compressive. It has been thought that the normal stress becomes tensile at points very close to the tool [18]. It is not possible to estimate such a point where the stress changes direction without making an assumption about the normal stress distribution on the boundary BC. Further analysis to study how k varies with both edge radius and rake angle is continuing. Figure 8 shows that the shear stress increases with decreasing uncut chip thickness. The reasons for this increase are related to strain and strain-rate hardening.

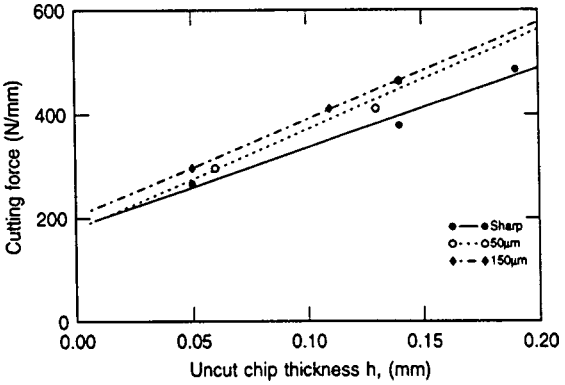

Fig. 5 Cutting force component versus uncut chip thickness for 70-30 brass [$\gamma_o = -5$ deg, $V = 7.8$ mm/s]

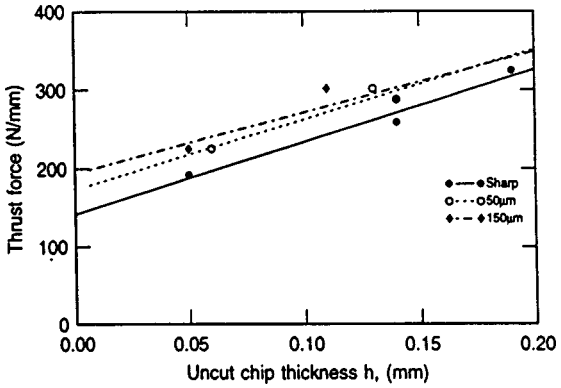

Fig. 6 Thrust force component versus uncut chip thickness for 70-30 brass [$\gamma_o = -5$ deg, $V = 7.8$ mm/s]

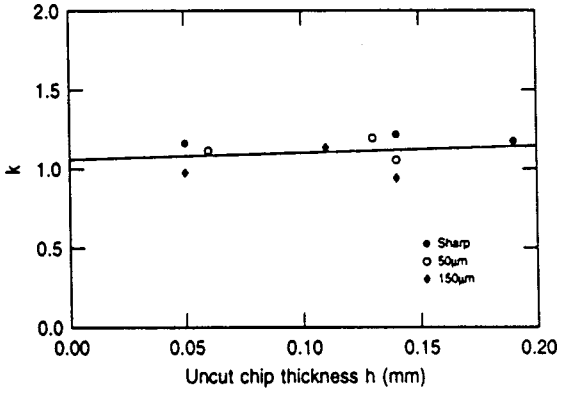

Fig. 7 Calculated normal stress factor k versus uncut chip thickness [$\theta = 30$ deg, $\psi = 20$ deg]

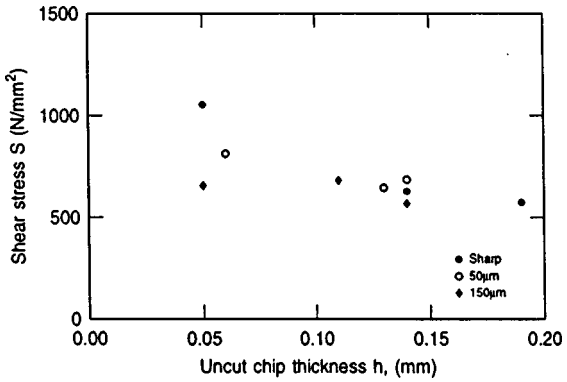

Fig. 8 Calculated shear stress versus uncut chip thickness [$\theta = 30$ deg, $\psi = 20$ deg]

In terms of strain, the results computed using the model indicate that the average strain for each of the conditions in these tests did not change significantly (less than 10 percent variation, except for the test at the smallest uncut chip thickness with the largest edge radius). This can be explained on the basis of these two facts: (a) as the shear angle decreases, which is the primary cause of increased strain on the chip, the volume of material deformed below the tool becomes a relatively larger percentage of the overall deformation volume, and (b) the strain imposed on the work is usually less than the strain in the chip. As a result, when the strains are weighted, the average strain does not change significantly when the shear angle decreases, which explains why strain hardening was not readily visible in these tests.

In terms of strain rate, however, there is an increase in strain rate with decreasing uncut chip thickness due to the decrease in time it takes for the deforming material to cross through the smaller shear zone. This changing strain rate is captured in Eq. (16). The strain rate is graphed versus uncut chip thickness in Fig. 9. It is seen that the strain rate increases exponentially with decreasing h . When shear stress and strain rates are plotted against

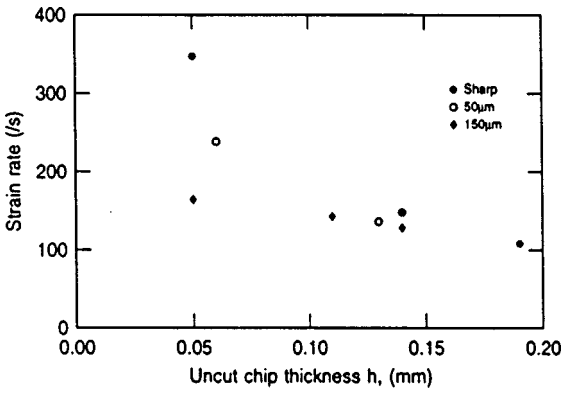

Fig. 9 Predicted shear strain rate versus uncut chip thickness [$\theta = 30$ deg, $\psi = 20$ deg]

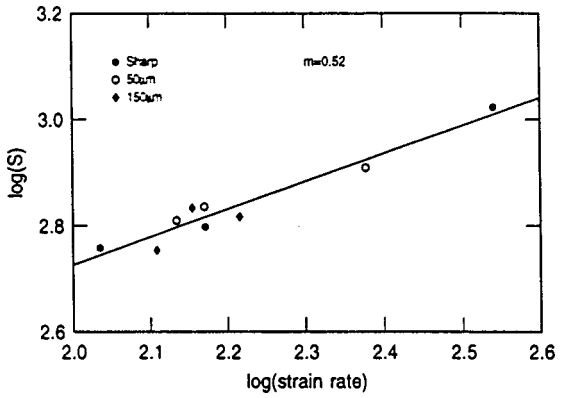

Fig. 10 Log(S) versus Log($\dot{\gamma}$) [θ=30 deg, ψ=20 deg]

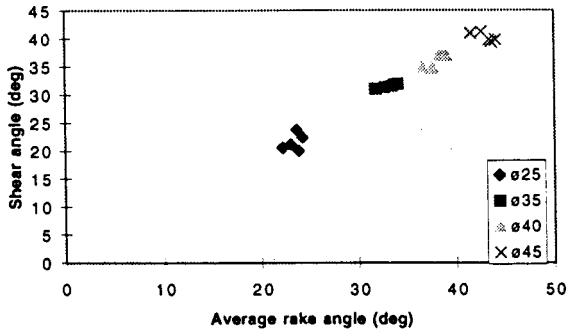

Fig. 11 Shear angle versus average rake angle for θ=50 deg. Machining data from Thomsen et al. [14].

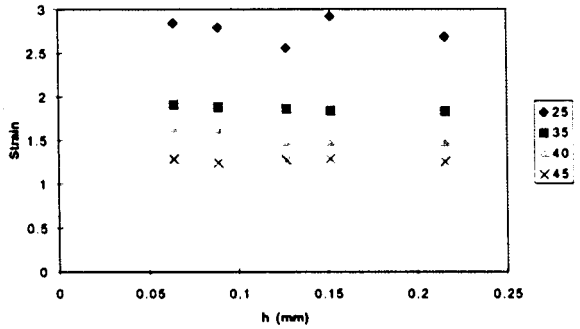

Fig. 12 Changing strains with tools of different rake angle. Machining data from Thomsen et al. [14].

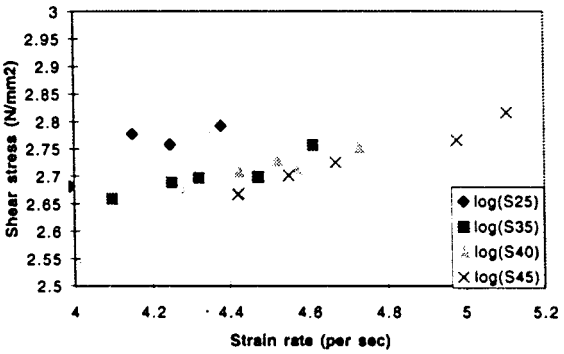

Fig. 13 A log-log plot of shear stress versus shear strain rate for θ=50 deg and ψ=20 deg. Machining data from Thomsen et al. [14].

each other on a log-log scale in Fig. 10, it shows that all the tools exhibit very similar strain rate sensitivities of $m=0.52$. The constant strain rate sensitivity shown indicates that the model meets the requirement proposed by Stevenson [24] and Schimmel et al. [25] that any model is ''good'' only if it exhibits consistency in its material constitutive relation, including $\dot{\gamma}$ effects. Changing the value of ψ does not significantly change the value of shear stress or the strain rate sensitivity. A change in ψ moves the line in Fig. 10 in the horizontal direction only.

Finally, regarding the work material, tensile tests at low strains and strain rates do indicate that brass is more sensitive to strain than strain rate. Despite this, the results here show that the primary reason for the increase in shear stress is strain rate sensitivity. This is not alarming since the variation in strain across test conditions was too low to observe noticeable strain hardening, as noted above. Furthermore, it should be noted that the shear stress S here is not intended to be identical to that of a tensile test but rather a property of the material during cutting.

The small amount of deviation of the data points is considered a very good result considering the following. First, the model is relatively simple. Second, no explicit selection of a shear zone size is necessary—only the selection of θ and ψ is needed, which, along with h, r_n and ϕ, dictates the shear zone size that is necessary for the calculation of the shear strain rate. Selection here of θ and ψ as set values is supported by a sensitivity study that confirmed insensitivity to these two parameters. The cause of the insensitivity can be explained since the relative change in shear zone size caused by changes in uncut chip thickness or edge radius is far more important than the absolute shear-zone size.

Analysis II. Thomsen et al. [14] present machining force and chip measurement data while cutting mild steel tubes with four HSS tools with nominal rake angles of 25, 35, 40 and 45 deg at a speed of 27 m/min (90 fpm). The uncut chip thickness in these experiments was varied from approximately 0.05 mm to 0.25 mm. No data regarding the edge radius on the tool was given except to say the tools were ground sharp before each test. An edge radius of 5 μm (0.0002 in) is assumed to correspond to the sharp tools that were used.

Shear angle was computed from the chip ratio data provided in Thomsen et al. [14]. Shear angle thus obtained is plotted versus average rake angle in Fig. 11. Since the assumed edge radii of the tools used are much smaller compared to the uncut chip thickness used, the average rake angle is nearly the same as the nominal rake angle. Hence, there is very little spread in the average rake angle for each tool.

The strains that are imposed by different rake angle tools should be expected to be different. It can be seen in Fig. 12 that the strain in the process decreases with increasing rake angle. It should also be noted that the strain does not change appreciably with uncut chip thickness for each tool. This is to be expected since changing h minimally affects the shape of the shear zone and mainly affects the size of the shear zone and hence strain rate only.

Shear stress was computed using the same procedure described previously and is plotted versus strain rate on a log-log scale in Fig. 13. It is seen that the material exhibits similar strain rate sensitivity for the different rake tools. The shear stress increases with decreasing positive rake angle (and increasing strain as seen in Fig. 12). Thus, the material is both strain and strain rate sensitive. Since all the tests were run at the same speed, it could be assumed that the effect of temperature on shear stress is constant. In this case, the shear stress of the material can be modeled as $S=S_0\gamma^n\dot{\gamma}^m$ [24]. The model parameters were estimated for the cutting conditions by conducting a linear regression in the log space and found to be

$$\log S = 1.86 + 0.33 \log \gamma + 0.18 \log \dot{\gamma}, \quad (34)$$

where the shear stress S has units of N/mm^2. The R^2 value for the fit was 77 percent and the standard error was 0.021 which is quite reasonable. This indicates the mild steel has a strain index of 0.33 and a strain rate index of 0.18. The results from the new model also indicate that the material behaves consistently when an accounting for the ploughing mechanism is made, as done in the new model, and the shear stress is modeled as a function of both strain and strain rate. It should be noted that no attempts have been made to correlate these values to the experimental tensile test data since the shear stress S is not intended to be identical to the values obtained from a tensile test. Nevertheless, the method does show the potential for evaluating properties of a material during cutting and shows that the property is consistent within the domain of the process of cutting metal.

Conclusions

Several qualitative observations and results from the metal cutting literature have been used to develop a new orthogonal process model that explicitly includes the effects of the edge radius. By conducting a force balance on the lower boundary of the deformation zone, a machining force model has been developed. Analysis of experimental data demonstrates the following points regarding the model and its behavior.

- The increase in specific energy with edge radius is not only due to the energy dissipated in deforming the machined surface but also due substantially to the energy expended in shearing the chip, as introduced by a more negative average rake angle.
- Increase in specific energy is also due to increases in strain and strain rate, which is another cause for size effect.
- Material, as characterized by the shear stress S via analysis under the new model, exhibits constant strain and strain rate sensitivity across edge radii and uncut chip thickness. This consistent constitutive material behavior is taken as a measure of the ''goodness'' of the machining force model, as proposed by Stevenson [24] and Schimmel et al. [25].

References

[1] Schimmel, R. S., Manjunathaiah, J., and Endres, W. J., 2000, ''An Experimental Investigation of the variability of Edge Hones and Their Effects on Machining Forces,'' to appear, ASME J. Manu. Sci. Eng.

[2] Bitans, K., and Brown, R. H., 1965, ''An Investigation of the Deformation in Orthogonal Cutting,'' Int. J. Mach. Tool Des. Res., **5**, pp. 155–165.

[3] Kita, Y., Ido, M., and Kawasaki, N., 1982, ''A Study of Metal Flow Ahead of Tool Face With Large Negative Rake Angle,'' J. Eng. Ind., **104**, pp. 319–325.

[4] Makino, R., and Usui, E., 1973, ''An Analysis of Stress and Strain Distributions in the Plastic Region of Slow Speed, Steady-State Machining,'' Bull. Jpn. Soc. Precis. Eng., **7**, No. 2, pp. 43–50.

[5] Manjunathaiah, J., and Endres, W. J., 1996, ''Effects of a Honed Cutting Edge in Machining,'' in *Proceedings of the Second S. M. Wu Manufacturing Symposium, Ann Arbor*, pp. 25–32, SME.

[6] Nakayama, K., and Tamura, K., 1968, ''Size Effect in Metal Cutting Force,'' J. Eng. Ind., **90**, pp. 119–126.

[7] Albrecht, P., 1960, ''New Developments in the Theory of Metal Cutting Process,'' J. Eng. Ind., **82**, pp. 348–358.

[8] Masuko, M., 1956, ''Fundamental Research on the Metal Cutting—Second Report,'' Bull. JSME, **22**, pp. 371–377.

[9] Abdelmoneim, M. Es., and Scrutton, R. F., 1974, ''Tool Edge Roundness and Stable Build-up Formation in Finish Machining,'' J. Eng. Ind., **96**, No. 4, pp. 1258–1267.

[10] Elanayar, S., and Shin, Y. C., 1996, ''Modeling of Tool Forces for Worn Tools: Flank Wear Effects,'' J. Manuf. Sci. Eng., **118**, pp. 359–366.

[11] Endres, W. J., DeVor, R. E., and Kapoor, S. G., 1995, ''A Dual Mechanism Approach to the Prediction of Machining Forces—Parts 1 & 2,'' J. Eng. Ind., **117**, pp. 526–542.

[12] Hsu, T. C., 1966, ''A Study of the Shear and Normal Stresses on a Cutting Tool,'' J. Eng. Ind., **88**, pp. 51–54.

[13] Okushima, K., and Kakino, Y., 1989, ''Study on the Generating Process of Machined Surface,'' Bull. JSME **12**, pp. 119–126.

[14] Thomsen, E. G., Lapsley, J. T., and Grassi, R. C., 1953, ''Deformation Work Absorbed by the Workpiece During Metal Cutting,'' Trans. ASME, **7**, pp. 591–603.

[15] Waldorf, D. J., 1996, *Shearing, Ploughing and Wear in Orthogonal Machining*, Ph.D. thesis, University of Illinois.

[16] Wu, D. W., 1988, ''Application of a Comprehensive Dynamic Cutting Force Model to Orthogonal Wave Generating Processes,'' Int. J. Mech. Sci., **30**, No. 8, pp. 581–600.

[17] Arsecularatne, J. A., 1997, ''On Tool-Chip Interface Stress Distributions, Ploughing Force and Size Effect in Machining,'' Int. J. Mach. Tools Manuf., **37**, No. 7, pp. 885–889.

[18] Connolly, R., and Rubenstein, C., 1968, ''The Mechanics of Continuous Chip Formation in Orthogonal Cutting,'' Int. J. Mach. Tool Des. Res., **8**, pp. 159–187.

[19] Oxley, P. L. B., 1989, *The Mechanics of Machining: An Analytical Approach to Assessing Machinability*, Ellis Horwood Limited.

[20] Hill, R., 1950, *The Mathematical Theory of Plasticity*, Clarendon, Oxford.

[21] Basuray, P. K., Mishra, B. K., and Lal, G. K., 1977, ''Transition From Ploughing to Cutting During Machining With Blunt Tool,'' Wear, **43**, pp. 341–349.

[22] Kragelskii, I. V., *Friction and Wear*, 1965, Butterworths, London.

[23] Komanduri, R., 1971, ''Some Aspects of Machining With Negative Rake Tools Simulating Grinding,'' Int. J. Mach. Tool Des. Res., **11**, pp. 223–233.

[24] Stevenson, R., 1997, ''Study on the Correlation of Workpiece Mechanical Properties From Compression and Cutting Tests,'' Mach. Sci. Technol., **1**, No. 1, pp. 67–70.

[25] Schimmel, R. S., Stevenson, R., and Endres, W. J., 2000, ''Application of an Internally Consistent Material Model to Determine the Effect of Tool Edge Geometry in Orthogonal Machining,'' to appear, ASME J. Manuf. Sci. Eng.